



# **JGR Space Physics**

# RESEARCH ARTICLE

10.1029/2022JA030541

#### **Key Points:**

- The temporal evolution of the 2-D strip-like bulge is recorded on gridded total electron content (TEC) maps
- The strip-like bulge is a consequence of the narrowing midlatitude band structure driven by the disturbance neutral wind
- The enhanced equatorial fountain effect is not involved during the formation of the strip-like bulge

#### Correspondence to:

J. Zhong, zhongjh55@mail.sysu.edu.cn

#### Citation:

Wan, X., Zhong, J., Zhang, S.-R., Xiong, C., Wang, H., Liu, Y., et al. (2022). Disturbance neutral winds effects on the ionospheric strip-like bulge at lower-middle latitudes. *Journal of Geophysical Research: Space Physics*, 127, e2022JA030541. https://doi.org/10.1029/2022JA030541

Received 8 APR 2022 Accepted 30 JUN 2022

#### **Author Contributions:**

Conceptualization: Xin Wan Formal analysis: Xin Wan, Jiahao Zhong, Chao Xiong, Yongqiang Hao Funding acquisition: Hui Wang, Fuqing Huang, Qiaoling Li, Jiawei Kuai Investigation: Xin Wan, Shun-Rong Zhang

Methodology: Xin Wan

**Project Administration:** Xin Wan,

Jiahao Zhong Resources: Xin Wan

Software: Xin Wan Supervision: Jiahao Zhong Validation: Xin Wan, Jiahao Zhong,

Yongqiang Hao

Visualization: Xin Wan Writing – original draft: Xin Wan Writing – review & editing: Xin Wan, Jiahao Zhong, Shun-Rong Zhang, Chao Xiong, Hui Wang, Yiwen Liu, Fuqing

Huang, Qiaoling Li, Jiawei Kuai, Jiawen

Chen, Yongqiang Hao

© 2022. American Geophysical Union. All Rights Reserved.

# Disturbance Neutral Winds Effects on the Ionospheric Strip-Like Bulge at Lower-Middle Latitudes

Xin Wan<sup>1,2</sup>, Jiahao Zhong<sup>1,2</sup>, Shun-Rong Zhang<sup>3</sup>, Chao Xiong<sup>4,5</sup>, Hui Wang<sup>4</sup>, Yiwen Liu<sup>6</sup>, Fuqing Huang<sup>7</sup>, Qiaoling Li<sup>8</sup>, Jiawei Kuai<sup>9</sup>, Jiawen Chen<sup>1</sup>, and Yongqiang Hao<sup>1</sup>

<sup>1</sup>Planetary Environmental and Astrobiological Research Laboratory (PEARL), School of Atmospheric Sciences, Sun Yat-sen University, Zhuhai, China, <sup>2</sup>Key Laboratory of Tropical Atmosphere-Ocean System, Ministry of Education, Zhuhai, China, <sup>3</sup>Haystack Observatory, Massachusetts Institute of Technology, Cambridge, MA, USA, <sup>4</sup>Department of Space Physics, College of Electronic Information, Wuhan University, Wuhan, China, <sup>5</sup>Hubei Luojia Laboratory, Wuhan, China, <sup>6</sup>School of Physics and Electronic Information, Shangrao Normal University, Shangrao, China, <sup>7</sup>CAS Key Laboratory of Geospace Environment, School of Earth and Space Sciences, University of Science and Technology of China, Hefei, China, <sup>8</sup>School of Space Science and Physics, Shandong Key Laboratory of Optical Astronomy and Solar-Terrestrial Environment, Institute of Space Sciences, Shandong University, Weihai, China, <sup>9</sup>College of Astronautics, Nanjing University of Aeronautics and Astronautics, Nanjing, China

**Abstract** During the geomagnetic storm on 3–6 November 2021, the in-situ plasma density and the gridded total electron content (TEC) maps registered a persistent presence of the strip-like bulges (electron density enhancement, also known as the shoulders in previous literatures) at lower-middle latitudes. The observed strip-like bulge resided in the Pacific-America-Atlantic sector and lasted from 07:00 UT on 4 November to 20:00 UT on 6 November. For the first time, the temporal evolution of the 2-D strip-like bulge was recorded by gridded TEC maps, though observations were limited over the North American continents. The TEC maps showed a continuous shrinking of the nightside midlatitude plasma band structure right before the presence of the narrow strip-like bulge. Simultaneous measurements from the Ionospheric Connection Explorer satellite (ICON) revealed an equatorward turning of the field-aligned ion transportation driven by the disturbance equatorward neutral winds. However, the enhanced fountain effect at low latitudes was not observed during the entire formation phase of the strip-like bulge. We propose that the storm-induced enhanced equatorward thermospheric neutral winds push the plasma equatorward along the field lines, and the plasma band structure was developed into the strip-like bulge. In addition, the ion composition of both the plasma band structure and the strip-like bulges are dominated by  $H^+$ , and the maintenance of the strip-like bulge could be due to the compensation of the downward plasmaspheric content flux.

# 1. Introduction

An important aspect of the ionospheric behaviors during geomagnetic storms is the occurrence of various kinds of intermediate-scale plasma density structures at different latitudinal sectors. A brief list of those structures includes the tongue of ionization (e.g., Coster et al., 2007; Foster et al., 2005; Zhang et al., 2021) and plasma patches (e.g., Xiong, Lin, et al., 2019; Zhang et al., 2013) at high latitudes, storm enhanced density (SED) at upper-middle latitudes of about 40°~60° magnetic latitudes (Foster, 1993; Zhang et al., 2017), and enhanced or depressed equatorial plasma bubble (EPB) activities at low and equatorial latitudes (e.g., Aa et al., 2018; Carter et al., 2016; Wan et al., 2018; Yeh et al., 2001). Those intermediate-scale ionospheric structures could be served as a screen to monitor the complex solar wind-magnetosphere-ionosphere-thermosphere coupling under different solar wind and geomagnetic field configurations. In the meantime, the sharp plasma density gradients of those structures would affect the radio signal transmission significantly, and particularly, pose threat to various global navigation satellite systems (GNSS) applications (e.g., Carter et al., 2014; Xiong et al., 2016; Xiong, Lin, et al., 2019; Zakharenkova & Cherniak, 2021). Hence, extensive studies that focus on the detailed dynamics of those intermediate scale ionospheric structures at specific latitudes had been carried out.

Nevertheless, the lower-middle latitudes  $(30^{\circ} \sim 45^{\circ})$  magnetic latitude), where the plasma density transit from a high level at low latitudes to a low level at middle latitudes, seems to attract far less attention. In previous studies that concern the ionospheric response to the geomagnetic storm, this latitudinal range appears as either the source region where the plasma is transported poleward and contributes to SED (Foster et al., 2007; Kelley et al., 2004; Vlasov et al., 2003) or the drain of the enhanced equatorial fountain effect (Foster & Coster, 2007;

WAN ET AL. 1 of 17



Foster et al., 2007; Mannucci et al., 2005; Tsurutani et al., 2004), which might further bring in the extended EPBs (Aa et al., 2018; Zakharenkova & Cherniak, 2020) during geomagnetic storms.

However, a local intermediate-scale structure called "shoulders" had long been noticed by Tsurutani et al. (2004) and Mannucci et al. (2005) during a few super geomagnetic storms. The shoulders appear as narrow plasma density bulges with clear poleward boundary and reside at conjugate lower-middle latitudes as seen in the meridional profiles of total electron content (TEC) (Mannucci et al., 2005; Tsurutani et al., 2004) or the in-situ plasma density (Heelis & Coley, 2007). Together with the aid of regional TEC maps, the shoulders had then been witnessed from time to time (Foster & Erickson, 2013; Foster et al., 2007; Horvath & Lovell, 2008), but only a few dedicated works had been carried out (Chartier et al., 2021; Datta-Barua et al., 2008; Foster & Coster, 2007; Maruyama et al., 2013; Wan et al., 2021).

Foster et al. (2007) and Foster and Coster (2007) first reported the shoulders in a form of localized enhancement in regional TEC maps in the American sector. Maruyama et al. (2013) observed a similar localized enhancement in Japan and further inferred its northwestward streaming nature. Datta-Barua et al. (2008) found that the electron content above 700 km has a considerable contribution to the localized TEC enhancement. A recent work that combines the data assimilation with a numerical model (Chartier et al., 2021) had also captured the shoulders as a regional ridge-like enhancement that extends in the zonal direction and estimated the GNSS positioning errors induced by the structure. Note that in the abovementioned works, the shoulders (or the so-called localized enhancement) were all observed at post-sunset hours with limited spatial coverage, hence, it was mainly recognized as a regional nighttime phenomenon.

Recently, by utilizing six high inclinations low earth orbit (LEO) satellites that flew at multiple local time sectors during the 8–9 September 2017 geomagnetic storm, Wan et al. (2021) had advanced the current understanding of the shoulders in various aspects: (a) The shoulder is indeed a local time independent phenomenon, though it is seen more evident in the nightside. (b) Its zonal extension exceeds  $150^{\circ}$  in longitudes, while its meridional scale is only a few degrees in latitude. (c) It lasts for more than 2 days throughout the storm recovery phase. (d) At 840 km,  $O^+$  is not involved in forming the shoulders, instead, the plasmaspheric ions of  $H^+/He^+$  are the only contributors, suggesting their plasmaspheric nature. These new findings revealed that the shoulder could be recognized as a snapshot of the strip-like structure with a narrow meridional coverage but extremely wide zonal extension. Besides, though the strip-like bulge could be categorized as the shoulders, for those shoulders without a clear equatorward boundary and attached to the SED plume, they are not equivalent to the strip-like bulge which resides far away from SED plume. Moreover, in this earlier study, the gridded TEC maps provided by Haystack Observatory of the Massachusetts Institute of Technology (MIT) failed to capture the phenomenon, and thus the detailed temporal evolution of the strip-like bulges was left unknown.

Previous studies pointed out that, accompanied by the shoulders, expanded equatorial ionization anomaly (EIA) was frequently observed at low latitudes (e.g., Mannucci et al., 2005; Tsurutani et al., 2004), indicating a possible relationship between these two phenomena. Hence, the enhanced eastward electric field that facilitates stronger fountain effects to produce expanded EIA was also frequently referred to as a possible formation mechanism of the shoulders (Chartier et al., 2021; Foster & Coster, 2007; Mannucci et al., 2005; Maruyama et al., 2013; Tsurutani et al., 2004). However, this mechanism is far from sufficient. That is, the plasma content convergence in a flux tube should exist to form the narrow bulges (in meridional dimension) via shaping its sharp poleward and equatorward boundaries, but the enhanced fountain effect itself cannot induce this convergence as it would cascade the plasma down to the middle latitudes in a rather smooth way via diffusion. The numerical simulations suggest that the enhanced eastward electric field alone is not adequate to produce the observed EIA features, and the effects of the enhanced equatorward neutral wind (e.g., Emmert et al., 2001; Fejer et al., 2000; Wang et al., 2017; Xiong et al., 2015) must be involved (Balan et al., 2010; Lin et al., 2005), as the latter term would reduce (or stop) the downward diffusion of plasma along the geomagnetic field lines, lift the ionosphere to a high altitude, and hence accumulate the plasma due to the low chemical loss. Similarly, equatorward disturbance neutral winds could also be a plausible driver for the appearance of the bulges by stopping the downward diffusion of plasma at lower-middle latitudes and shaping the sharp poleward boundary of the bulges (Wan et al., 2021). Nevertheless, this mechanism needs more observations, such as direct measurements of neutral winds.

During the deep solar minimum of 2021, an intensive geomagnetic storm occurred on 3–6 November. This study shows that multiple high-inclination LEO satellites had persistently captured the signatures of the strip-like bulge

WAN ET AL. 2 of 17



near the dawn-dusk terminator. Moreover, the low background ionospheric plasma density made the strip-like bulge distinguishable on the gridded regional TEC maps, allowing a full record of the detailed temporal evolution of the strip-like bulge. Together with both the neutral and ionized particle measurements made by the Ionospheric Connection Explorer (ICON) satellite, the formation mechanisms associated with disturbance thermospheric neutral wind and enhanced fountain effect are examined.

# 2. Data Description

In-situ plasma densities measured by five high-inclination satellites of Swarm A, Swarm B (Friis-Christensen et al., 2008), and Defense Meteorological Satellite Program (DMSP) F16, F17, F18, are used to extract the bulge signatures. Swarm A and B are near-polar (87° inclination) orbiting satellites, and their onboard Langmuir probes provide ion density (*Ni*) measurements with 2 Hz sampling rate. DMSP satellites fly in sun-synchronous orbits (98.7° inclination) at altitudes around 840 km, and each satellite carries a suite of sensors to measure the densities, temperatures, and drift motions of ionospheric ions or electrons. The ion drift motion is measured with three components: ram drift, vertical crosstrack drift, and horizontal crosstrack drift. The 13th generation of the International Geomagnetic Reference Field (IGRF-13, Alken et al., 2021) is adopted to derive the ion drift components in the geomagnetic frame. During the periods of interest, Swarm and DMSP satellites flew in the dawn-dusk sector. Specifically, the equatorial crossing local time (LT) of Swarm A is in 05:30/17:30, Swarm B is in 05:40/17:40 LT, DMSP F16 is in 04:30/16:30 LT, DMSP F17 is in 06:30/18:30 LT, DMSP F18 is in 04:10/16:10 LT.

In addition, the 2-D gridded TEC map provided by the Massachusetts Institute of Technology's Haystack Observatory is used to supplement the satellite observations. The data set has a spatial resolution of  $1^{\circ} \times 1^{\circ}$  (latitude × longitude) and a time resolution of 5 min (Rideout & Coster, 2006).

The ICON (Immel et al., 2018) is a low-inclination (27°) LEO satellite that orbits the earth at approximately 580 km and provides multiple types of observations associated with both neutral and ionized particles obtained by the payloads of Michelson Interferometer for Global High-Resolution Thermospheric Imaging (MIGHTI, Harding et al., 2017) and Ion Velocity Meter (IVM, Heelis et al., 2017), respectively. MIGHTI instrument employs two separate sensors: MIGHTI-A and MIGHTI-B, to observe the airglow of both the red- and green-line oxygen emissions in two orthogonal directions in azimuth of 45° and 135° from the spacecraft ram direction. Each interferometer acquires altitudinal distribution of line-of-sight (LOS) wind velocity in an altitude range of 150~300 km. It takes about 5~8 min for the MIGHTI-B to revisit approximately the same location as the MIGHTI-A has visited. Hence, two orthogonal LOS wind components can be derived at each tangent point in 5~8 min, and with the assumption that the thermospheric wind does not change during this time interval, the wind vector can be obtained. ICON IVM consists of two planar sensors of a retarding potential analyzer and an ion drift meter to measure the ion density, ion temperature, ion composition, and ion drift velocity. To monitor the background state of the neutral and ionized particles, we used the ICON level 2 MIGHTI Cardinal Vector Winds data set and level 2 IVM-A data set. Particularly, the investigated phenomenon is primarily found above 430 km by the aforementioned LEO satellite, so we only use the ICON neutral winds data in altitudes of 250~300 km, which is closer to the other observations.

# 3. Geospace Conditions Associated With the Geomagnetic Storm

Figure 1 shows the geospace parameters during the period of 3–7 November 2021. The sudden storm commencement (SSC) occurred at about 21:00 Universal Time (UT) on 3 November. At the same time, the solar wind velocity increased abruptly and the interplanetary magnetic field (IMF) turned southward ( $B_z < 0$ ). Afterward, the decrease of SYM-H implies the main phase, and  $B_z$  kept oscillating. Meanwhile, Kp increased intensively and reached a peak value of 7, when the SYM-H also dropped to a minimum value of -118 nT at 12:45 UT on 4 November. Finally, the recovery phase took over for the next few days.

WAN ET AL. 3 of 17



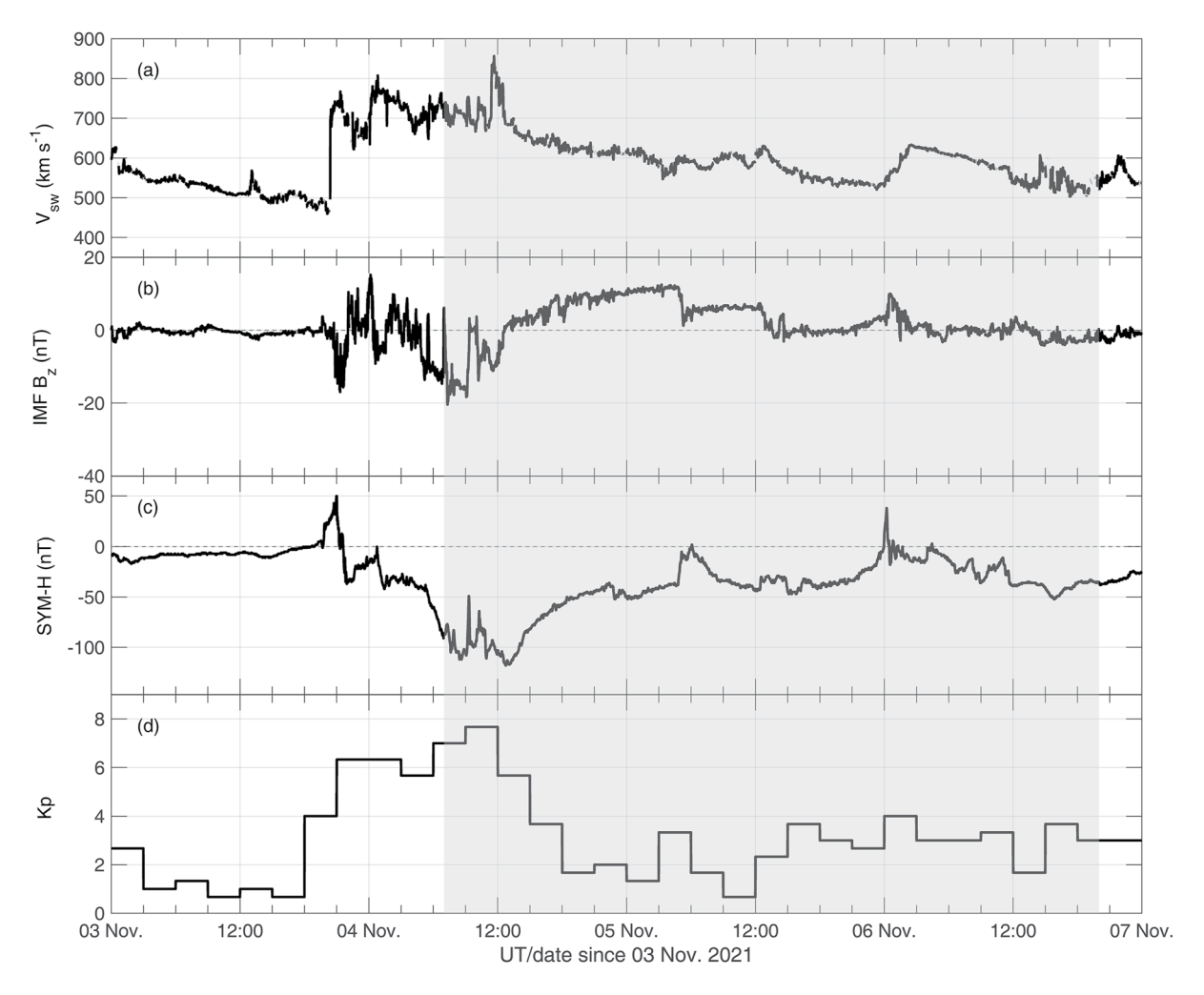


Figure 1. Variations of solar wind speed  $(V_{sw})$ , interplanetary magnetic field (IMF) component in the north-south direction  $(B_z)$ , and geomagnetic indices of SYM-H and Kp during  $3\sim7$  November 2021. The shaded area marks the period when the LEO satellites persistently snapshot the bulge signatures.

# 4. Results

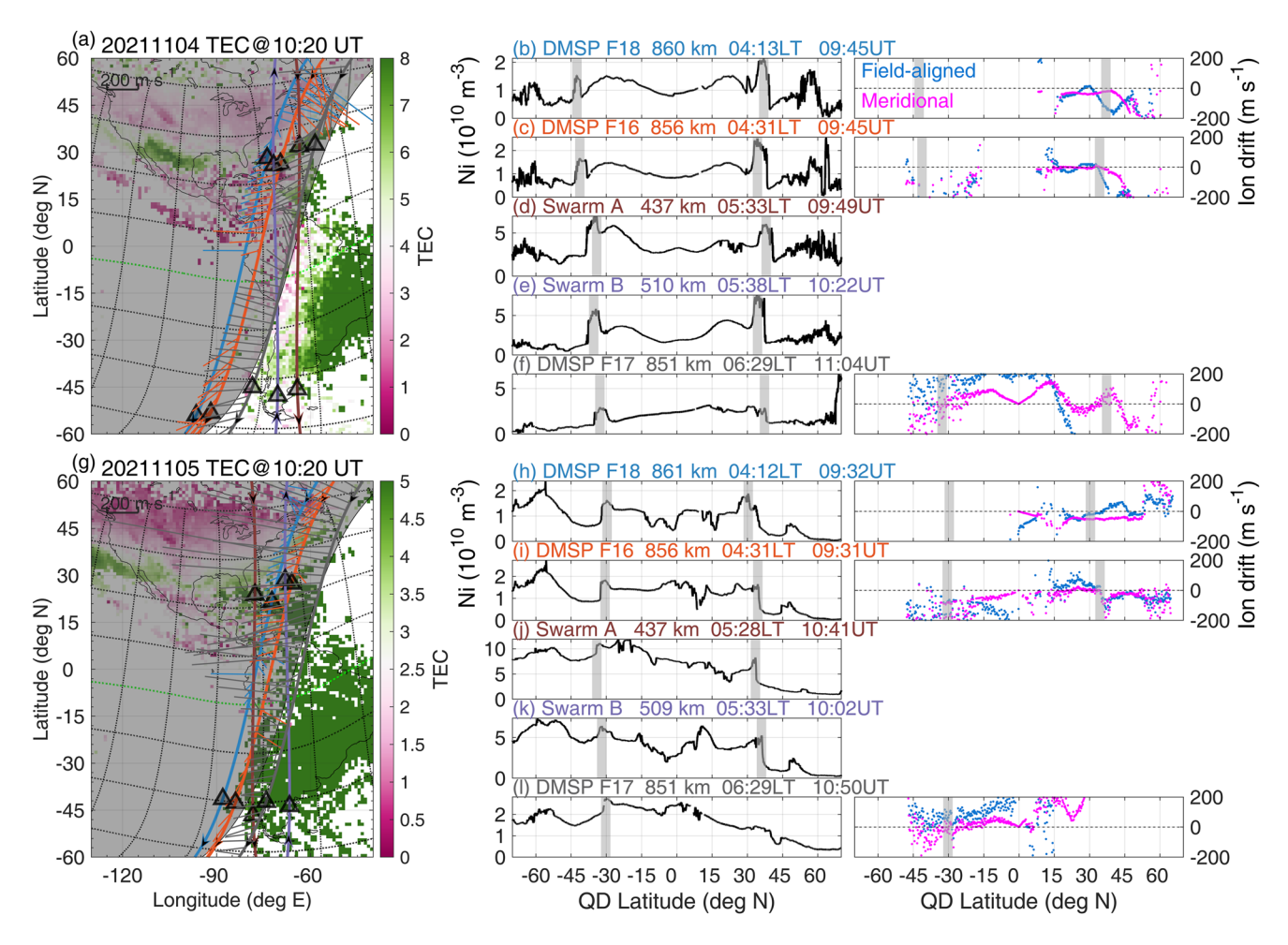
# 4.1. Plasma Density Bulges Seen in TEC Map and In-Situ Observations

Figure 2 presents two snapshots of the regional TEC map on 4 November and 5 November both at 10:20 UT, as well as the in-situ plasma density latitudinal profiles measured by five nearby LEO satellites. The trajectories of the satellites were shown on the TEC maps (Figures 2a and 2g). In North America, the TEC was generally maintained at a low level (lower than eight TEC units), but a ridge-like enhancement that spanned from the western Atlantic through the Gulf of Mexico to the west coast of the United States was witnessed. In the meantime, all the five satellites that flew near the sunrise terminator (only DMSP F17 was exposed to the sunlight region) had captured narrow plasma density enhancements (marked by triangles in Figure 2) with clear and sharp poleward boundary and equatorward boundary. The enhancements showed a width of about 5° in latitudes and were distributed at conjugate quasi-dipole (QD) latitudes of 30°~45°N/S, which are consistent with the strip-like bulges reported in Wan et al. (2021). In the northern hemisphere, those bulges resided well within the ridge-like TEC enhancements (Figures 2a and 2g). However, the southern bulges were distributed near the southern tip of the South American continents where the TEC data are sparse. Thus, how the southern bulges look on the local TEC map remains unknown.

On both days, the zonal ion drifts recorded by three DMSP satellites (left panels in Figure 2) were mainly westward near the strip-like bulge. However, on 4 November, clear drift shear appeared on the north of the strip-like bulge at dip latitudes of approximately 40°N (Figure 2a). Above the latitudes of the drift shear, the eastward ion

WAN ET AL. 4 of 17





**Figure 2.** Two clear registrations of strip-like bulge features by total electron content (TEC) maps on (a) 4 November and (g) 5 November at the same UT of 10:20. The dark dash lines are the magnetic meridian and QD latitudes; the QD latitudes are organized in a step of 15° with the magnetic equator marked in green color. The nearby trajectories of the five LEO satellites are attached to the maps, the stems on the trajectories are the horizontal ion drift vectors of DMSP satellites. The solid arrows mark the moving direction of the spacecraft. The corresponding *Ne/Ni* profiles, as well as the ion drift in the geomagnetic frame (the projection is calculated based on IGRF13, blue is field-aligned component: positive along the geomagnetic field vector; magenta is meridional component: within the geomagnetic meridional plane, perpendicular to the field line, positive outward), are shown on the right side (b–f, h–l). The dark shaded areas highlight the bulges which were further marked as transparent triangles in (a, g).

drift velocity increased with increasing latitudes (Figure 2a). The meridional ion drifts were mainly southward near the bulges in both hemispheres. Since the ion transportation is constrained by the geomagnetic field lines, we further showed the line plots of the ion drift in geomagnetic frame in right-most panels of Figure 2. Focus on the bulges, on 4 November, the field-aligned ion drifts were negative and positive in the northern and southern hemisphere, respectively, correspond to a consistent field-aligned equatorward ion transportation. The meridional drifts are mainly weakly negative near the bulge, except for the measurement of DMSP F17 in the northern hemisphere, suggesting an unfixed  $E \times B$  drift pattern. On 5 November, both the field-aligned and the meridional components varies in three DMSP orbits, which means the drifts are not uniformed among those bulge cases.

As the LEO satellites continuously orbited the earth, one can check the longitudinal extension of the plasma density bulges. To clarify the spatial and temporal distribution of those in-situ bulges, we have manually extracted the bulge cases from the five adopted LEO satellites during 4~6 November 2021. The distributions of the bulges as a function of longitude and UT in both hemispheres are shown in Figure 3. The interhemispheric distribution of the bulges is similar to the results reported in Wan et al. (2021), that the bulge cases are formed as two conjugate strips. The difference is that, in the case of 7~8 September 2017, the eastern end of the strip merely reached the west coast of the United States, but during this storm event, the strip had extended more eastward beyond the entire American sector and reached the middle Atlantic. For the temporal variations, the first bulge

WAN ET AL. 5 of 17



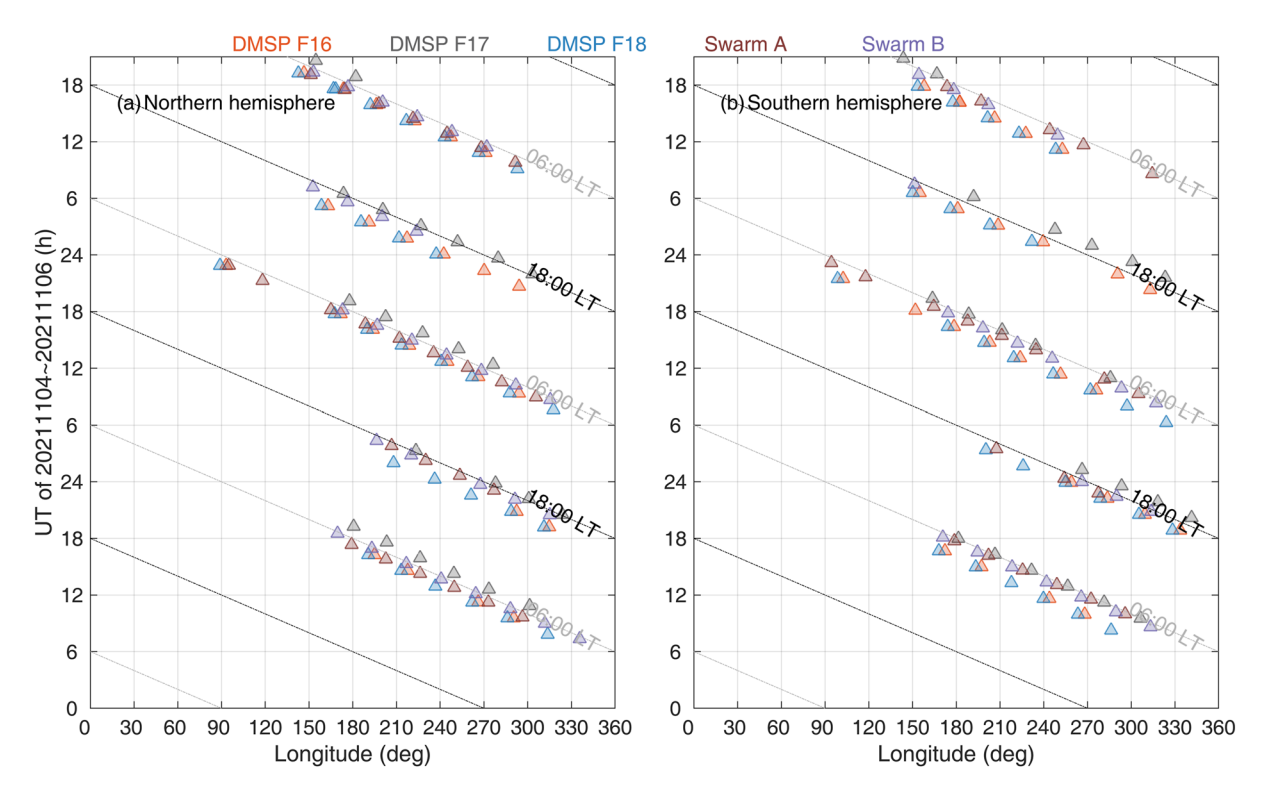


Figure 3. Distributions of the bulges snapshotted by five satellites, as a function of longitude and UT for (a) northern and (b) southern hemispheres. Dark black lines denote the local time of 18:00, gray lines denote the local time of 06:00.

was identified by Swarm B over the middle Atlantic Ocean at about 07:00 UT on 4 November. Since then, more bulges persistently appeared in conjugacy at the western longitudes and lasted for more than 2 days till 20:00 UT on 6 November. The time interval of the bulges' presence is shadowed in Figure 1, showing the period that lasted from the later hours of the main phase through the recovery phase.

# 4.2. Temporal Evolution of Strip-Like Bulges on TEC Maps

The above results provided a general picture of the strip-like bulges from multiple satellites' in-situ observations. However, the detailed temporal evolution of this giant two-dimensional structure remains unknown, and this cannot be resolved merely by satellite observation. Wan et al. (2021) had turned to regional TEC maps but they showed no bulge signatures during that 2017 event. Fortunately, in this case, the regional TEC maps shown in Figure 2a snapshotted part of this giant structure (the eastern part) in the dawn sector. Thus, the TEC map over the American sector may provide additional clues on the temporal evolution of the strip-like bulges, though not in a full resolution considering the structure could have zonal extension over 180° in longitude. Figures 4 and 5 presented TEC maps snapshotted over the American sector every 30 min during 03:00~14:30 UT on 4 November, and Figure 6 focuses on the time interval of 07:00~12:30 UT on 5 November.

At 03:00 UT on 4 November 2021 (Figure 4a), the TEC over the North American continents appeared as a giant patch (dark green) with an increasing gradient toward the east. Then the TEC patch shrank continuously during 03:30~07:00 on 4 November, 2021 (Figures 4b~4i), and the conjugate patch that spanned over the southern tip of the South American continent could be also identified. Meanwhile, the center part of the giant patch in the northern hemisphere exhibited a mild depletion that stretched from Central America to the northwest, and the patch transformed into a structure analogous to the crab pincer (flipped figure-C shape, most evident in Figure 4d). The first appearance of the northern strip-like bulge was then recorded at about 08:30 UT on 4 November 2021 (Figure 4i) as the green patch above the Gulf of Mexico shown in Figure 4l.

Afterward, as shown in Figure 5, the strip-like bulge was maintained persistently. Note that the conjugate position of the strip-like bulge in the southern hemisphere laid above the Pacific that the ground TEC data is not

WAN ET AL. 6 of 17



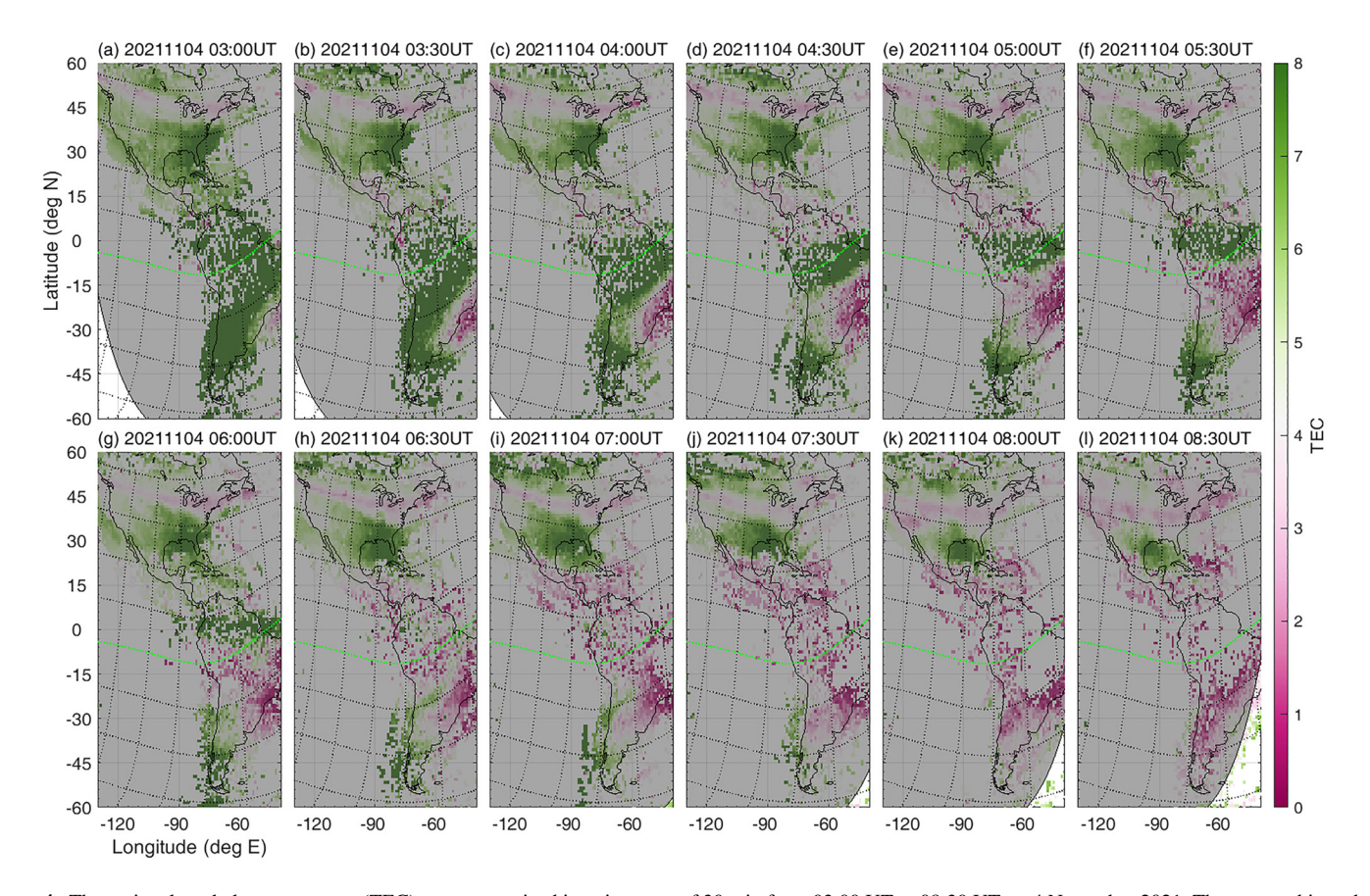


Figure 4. The regional total electron content (TEC) maps, organized in a time step of 30 min from 03:00 UT to 08:30 UT on 4 November 2021. The geographic and geomagnetic references are organized in the same way as Figure 2.

available, and we focus only on the northern hemisphere within this study. In Figures 5a~5h, the strip-like bulge exhibited a slight northwestward movement/extension. However, this movement/extension is slower than the west movement of the sunrise terminator, causing the sunlight illumination gradually approached the bulge structure over the American continent. As a result, the high TEC area caught up and finally masked the strip-like bulge (Figures 5i~5l). During the following daytime, the strip-like bulge cannot be identified on TEC maps (not shown).

Figure 6 shows the TEC maps during the next night  $(07:00\sim12:30 \text{ UT})$  on 5 November 2021. Before clear identification of the strip-like bulge during  $09:30\sim12:00 \text{ UT}$  (Figures  $6f\sim6k$ ), the TEC behaved as a greater (compared to the day before) "scraggy patch" that spans in  $15^{\circ}\sim40^{\circ}$  QD latitudes over the American sector (Figures  $6a\sim6e$ ). The emergence of the strip-like bulge is a result that the low latitude portion of this "scraggy patch" decayed, while its poleward border was generally unchanged, so it left a narrower strip behind. Afterward, the strip-like bulge became less visible, as the sunrise terminator approached and brought abundant TEC (Figure 61).

# 5. Discussion

The investigated period was during the solar minimum (F10.7 index is about 92 solar flux units), and all the adopted LEO satellites recorded an extremely low level of the plasma density of  $10^{10}$  m<sup>-3</sup> near the sunrise terminator. The low magnitude strip-like bulges can be identified on the nighttime TEC maps that the TEC is less than 8 TECU. As the TEC increased to a level of 50 TECU during the daytime, the strip-like bulge can no longer be identified (not shown). Besides, the nighttime TEC was at a higher level of 20 TECU in the case of 8–9 September 2017, and the bulge signature was still missed on TEC maps (Wan et al., 2021). Thus, it is inferred that the clear registration of strip-like bulge on TEC maps requires a low TEC background. We emphasize that though the recurring bulge signatures on satellite in-situ *Ni* profiles (in a time cadence equivalent to the orbital

WAN ET AL. 7 of 17



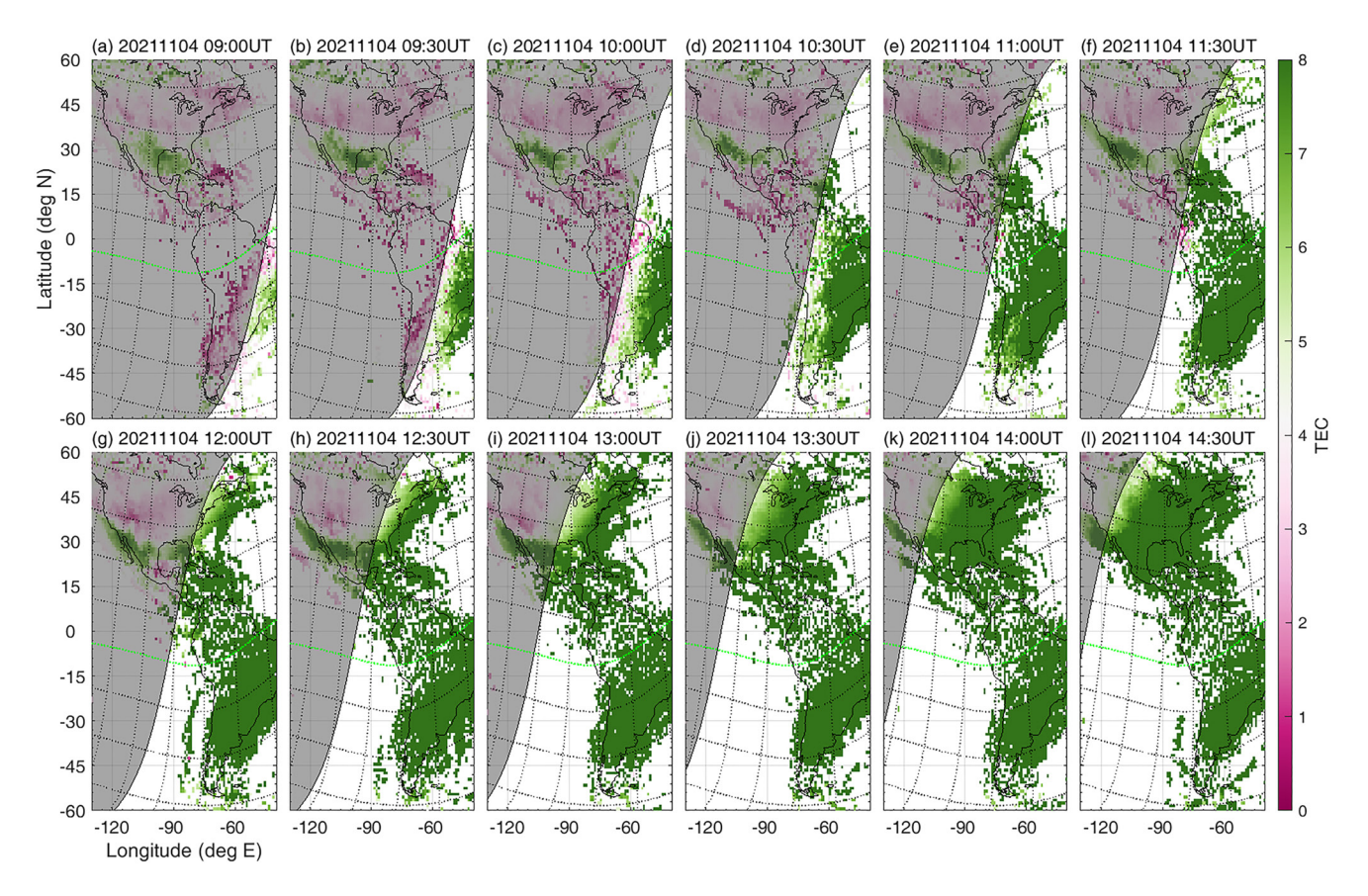


Figure 5. Same as Figure 4 but for the following UTs of 09:00~14:30.

period of approximately 90 min) are helpful to summarize its spatial-temporal distribution, the monitoring of the detailed evolution processes must be achieved by the continuous 2-D TEC maps. This may explain that though the phenomenon had been noticed by satellites from time to time, that is, during a few major storm events in higher solar activity years (Mannucci et al., 2005; Maruyama et al., 2013; Tsurutani et al., 2004), no in-depth dedicated observations had been reported. We suggest this geomagnetic storm during the solar minimum exposes the strip-like bulge more clearly to the community, leading to a better understanding of the phenomenon. Below, we will comparatively discuss the observed features of the formation and maintenance mechanisms of the strip-like bulge along with detailed reviews of previous studies.

# 5.1. Development of the Strip-Like Bulge

The above satellite observations of the strip-like bulges in this study are generally the same as that reported in the 7~8 September 2017 geomagnetic storm (Wan et al., 2021), though the local time coverages of the LEO satellites are different between the two cases. For the 2017 case, six satellite observations covered almost all the local time sectors (i.e., 10:00/22:00 LT for Swarm A, 03:30/15:30 LT for Swarm B, 02:30/14:30 LT for DMSP F15, 03:50/15:50 LT for DMSP F16, 06:30/18:30 LT for DMSP F17, 06:20/18:20 LT for DMSP F18) and the bulge signatures can be persistently identified at those LTs. During this event, all the five LEO satellites orbited the earth at the dawn-dusk sector, so that the presence of the bugles was only confirmed near the day-night terminator. The TEC maps filled the satellite observation gaps and confirmed the presence of strip-like bulges throughout the night, but the bulges' magnitude in TEC was too low to be identified from high TEC backgrounds during the day. Nevertheless, the recurring feature of the bulge in both dawn, dusk, and nighttime sectors in a 2-day time interval (Figure 3) strongly suggest that the local time independence should be a consistent feature, and the strip-like bulge shown in this event could be also survived in the daytime, following the results of Wan et al. (2021).

WAN ET AL. 8 of 17

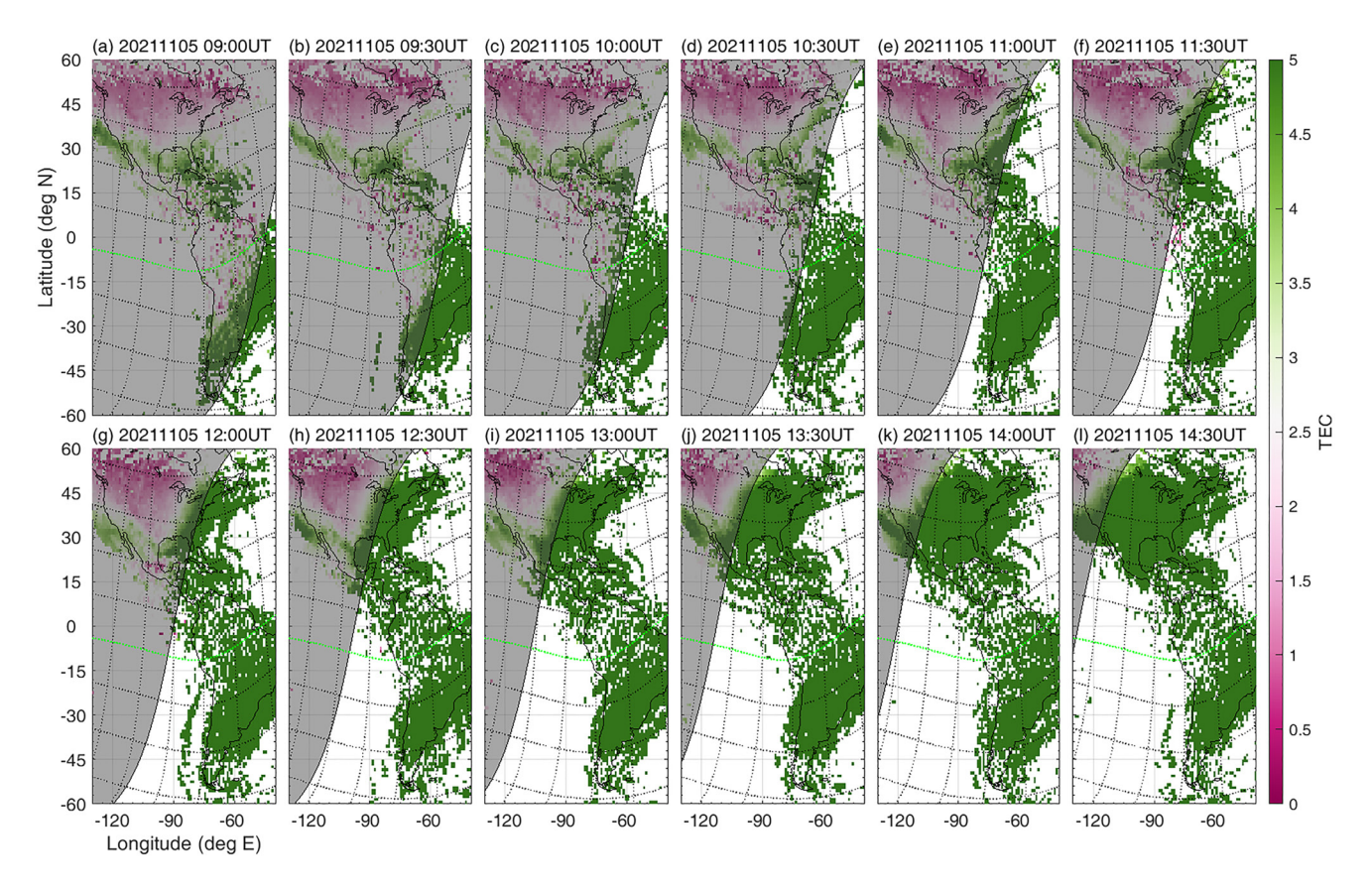


Figure 6. Same as Figure 4 but for the time interval of 07:00~13:30 UT on 5 November 2021.

On 4 November, satellite observations recorded the first appearance of the bulges at about 07:00 UT when the American sector was around midnight. The low background TEC offers the possibility for the TEC maps to reveal the full evolution of the strip-like bulges, in the American sector. Figures 4 and 5 show clearly that before the emergence of the strip-like bulge, the midlatitude ionosphere was dominated by the giant midlatitude patches consistently in the conjugate ionosphere. After the continuous erosion and shrinking, the patch gradually transformed into a strip-like bulge.

# 5.2. Nature of the Patch—Midlatitude Plasma Band Structure

The first issue is about the nature of the giant midlatitude patch. Note that the observed conjugate patch spans in the same latitude bins as that of the so-called midlatitude band structure (Zhong et al., 2019), which preferably appears during the night as hemispheric symmetric plasma density enhancements between  $\pm 30^{\circ}$  and ±50° magnetic latitudes, observed by Constellation Observing System for Meteorology, Ionosphere, and Climate (COSMIC) electron density (Ne) data. The same feature had also been noticed by COSMIC TEC, DMSP ion density, CHAllenging Minisatellite Payload (CHAMP) Ne, and Swarm Ne data (Li et al., 2018; Rajesh et al., 2016; Wan et al., 2020; Xiong, Lühr, et al., 2019). The middle-latitude band structure, also known as the midlatitude enhancement is assumed to be associated with the downward flux of plasmaspheric particles  $(H^+/He^+)$  due to the ambipolar diffusion (Zhong et al., 2019), though the detailed ion composition of the middle-latitude band structure had not been analyzed. In this study, supporting evidence of the ion composition of the middle-latitude band structure can be given by ICON IVM measurements, which will be presented in Figure 7 in Subsection 5.3. Besides, DMSP satellites also reveal that the strip-like bulge is predominantly formed by the light ions of  $H^+/He^+$ rather than  $O^+$  in Wan et al. (2021). Note that as the ion density of the bulge was greater in the topside ionosphere and showed enhanced H<sup>+</sup>, for the density profile at the same location, there might be greater ion density around the F2 peak with elevated  $O^+$ , which currently cannot be confirmed. The same dominance of  $H^+/He^+$  within the bulge is also applied to this event, though the ion composition observations from DMSP satellite are not shown.

WAN ET AL. 9 of 17



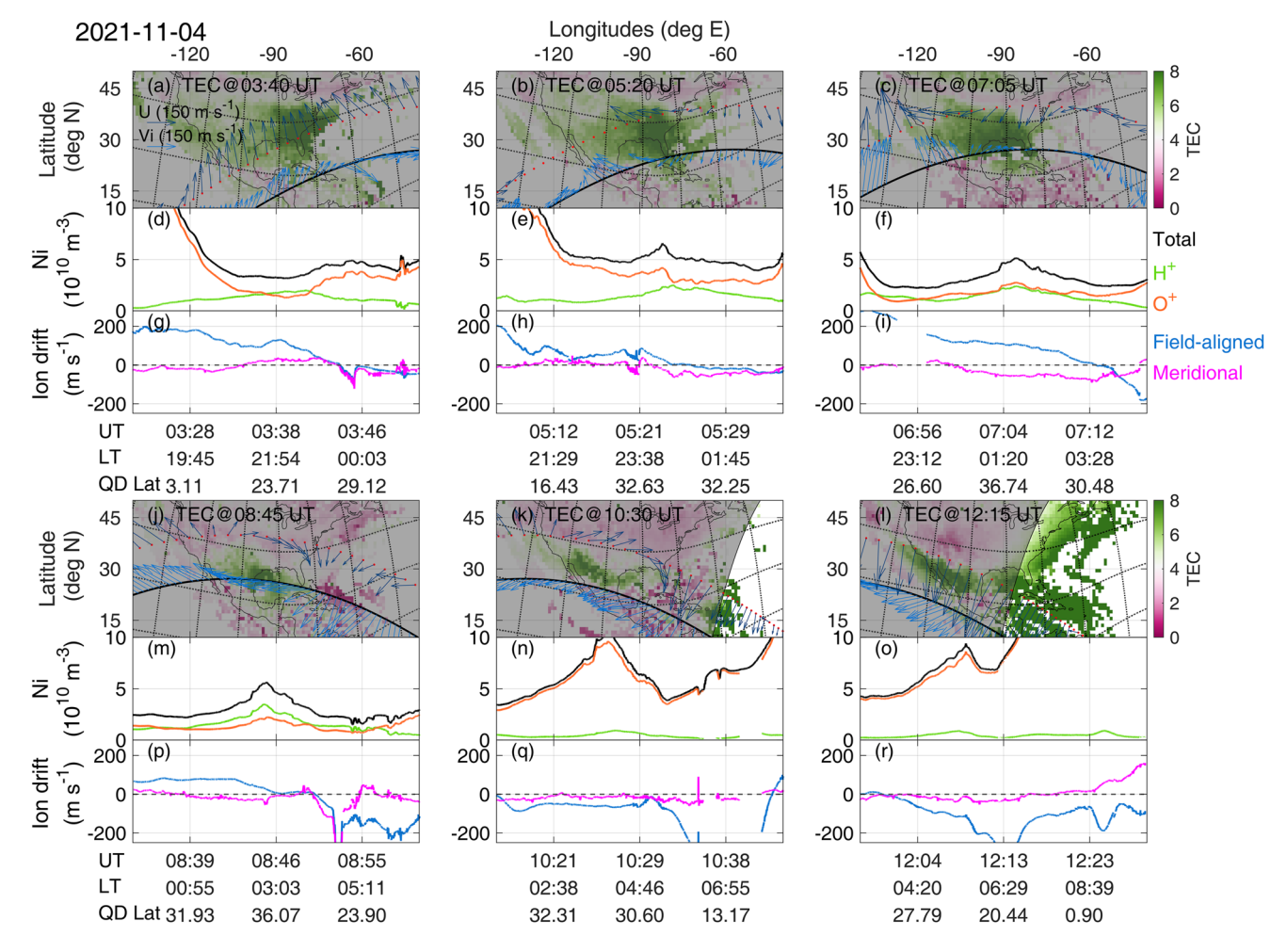


Figure 7. The total electron content (TEC) maps along with the plasma and neutral measurements made by ICON. (a–c, j–l) The geographic and geomagnetic references are organized in the same way as in Figure 2; Black solid lines and the red dots are the trajectories of the ICON and the tangent points seen from the onboard MIGHTI payload, respectively; The dark blue and light arrows denote the horizontal thermospheric wind (averaged for 250~300 km) and ion drift vector, respectively. (d–f, j–l) The along path total ion density (black),  $O^+$  density (orange), and  $H^+$  density (green). (g–i, p–r): The along path ion drift in the geomagnetic frame of the field-aligned (positive along the geomagnetic field vector) and meridional components (within the geomagnetic meridional plane, perpendicular to the field line, positive outward), colored in blue and magenta, respectively.

Thus, we believe the observed enhanced TEC patch is equivalent to the midlatitude band structure, and the strip-like bulge, to some extent, is the storm time mode of the midlatitude band structure. In the rest of the paper, we still refer to this TEC structure as the "patch" (or midlatitude patch), while the "bulge" describes the LEO observations on individual cases and the "strip-like bulge" generalizes the full morphology.

# 5.3. Disturbance Equatorward Neutral Wind Effects and Ion Composition

The second issue is about the driving forces that cause the shrinking of the midlatitude patch which led to the appearance of the strip-like bulge. The neutral winds could significantly push the plasma at lower altitudes and change the plasma pressure, then affect the plasma transportation along the magnetic field lines at the topside ionosphere. Figure 7 shows the ICON's observation of the F region horizontal neutral winds, ion drift vectors in geographic and geomagnetic frames, ion density, and ion compositions along with the six passes over North America. On 4 November, the TEC maps are presented as background. The black lines on geographic maps are the trajectories of the ICON, the red dots are the tangent points of the neutral wind observations in an altitude range of 250~300 km. The light blue and dark blue arrows represent the horizontal ion drift and neutral wind vectors, respectively.

WAN ET AL. 10 of 17



First, we focus on the region where the midlatitude patch and the strip-like bulge resided  $(-120^{\circ} \text{ to } -80^{\circ}\text{E})$ . At about 03:40 UT when the storm progressed to the main phase (Figure 1), both the horizontal ion drift and neutral wind exhibited poleward velocity near the TEC patch (Figure 7a). On the next orbit, the poleward velocities of both the neutral particle and ion are weakened around 05:20 UT (Figure 7b). At 07:05 UT, the neutral wind turned equatorward on the polar side of the giant patch, while the meridional component of the ion drift reached its minimum value (Figure 7c). Afterward (Figures 7j, 7k, and 7l), the equatorward components of the ion and neutral velocities exhibited continuous increases.

However, ICON measurements exhibited different evolution patterns over both the west side (−140°∼−110°E over Pacific) and east side (-80°~-40°E over Atlantic) of the patch. On the west side, the neutral wind remained poleward till 12:00 UT at pre-dawn, when it suddenly turned equatorward and ion drift evolved from strong poleward velocity to weak equatorward velocity. On the east side, both the meridional wind and meridional ion drift turned equatorward at 05:30 UT (Figure 7b) and were maintained throughout the following orbits. These two turnings occurred earlier by approximately 90 min (neutral wind, Figure 7c) and approximately 190 min (ion drift, Figure 7j) than that occurred in the vicinity of the TEC patch region, respectively. Thus, it can be concluded that the equatorward turnings of both the meridional neutral wind and ion drift launched first in the east (Atlantic) and then propagated to the west across the continent to the Pacific. And it takes a longer time for the ion drift to turn direction than the neutral wind to do so. Considering the spatial separation between the locations where the neutral wind and ion drift observations were made, it is reasonable to infer that the turning of the ion drift direction in the lower latitudes is motivated by the neutral wind disturbance propagation equatorward. Note that the turning of the meridional neutral wind happened at 05:30 UT (Figures 7b) and 07:00 UT (Figure 7c) over the Atlantic and the continent US, respectively. At the same time, the geomagnetic storm was in the main phase as the IMF Bz maintained southward, which enabled continuous dumping of solar wind energy into the magnetosphere-ionosphere-thermosphere system and led to the enhanced equatorward neutral wind disturbance.

To determine whether the inward  $E \times B$  drift or upward field-aligned drift is dominant, Figures  $7g\sim7i$ ,  $7p\sim7r$  additionally show the field-aligned (directed along the field line, blue) and meridional (perpendicular to field line and within the local magnetic meridional plane, magenta) components of the ion drift in the geomagnetic frame. It can be seen that the field-aligned ion drift decreased continuously and turned from positive (downward and poleward) to negative (upward and equatorward) after the emergence of the strip-like bulge (Figures 7p and 7q). Compared to the field-aligned components, the meridional ion drift was relatively weaker and had maintained negative before the appearance of the strip-like bulge (Figures 7h and 7i). Therefore, the upward/equatorward field-aligned ion drift was the dominant component during the turning.

Another interesting feature is that the first appearance of considerable equatorward ion drifts over the continent coincident with the first emergence of the strip-like bulge seen in TEC (Figure 7k). As for the Atlantic sector, the appearance of the considerable equatorward ion drift occurred at 07:15 UT (Figure 7c), though the TEC map was not available over there, DMSP F18 and Swarm B also coincidently registered the first bulge signal (Figure 3a). Besides, Figures 7b, 7c, and 7g show that as ICON flew closer to the patch, the ion composition of  $H^+$  exhibited a clear increase, while  $O^+$  did not. In Figure 7m, the  $H^+$  density even surpasses the  $O^+$  density. Moreover, the  $H^+$  density kept at a very low level as ICON flew outside of the strip-like bulge (Figures 7n and 7o). Those features confirmed the plasmaspheric source of the middle-latitude band structure (Li et al., 2018; Rajesh et al., 2016; Xiong, Lühr, et al., 2019; Zhong et al., 2019) as well as the strip-like bulge (Wan et al., 2021), and support the aforementioned inference that the strip-like bulge is likely the storm time pattern of the middle-latitude band structure. One should note that, Wan et al. (2021) had also shown that the  $O^+$  density could be still higher than the enhanced  $H^+$  density within the strip-like bulge at DMSP orbital altitudes. Therefore, although the  $H^+$  plays a dominant role in the appearance of the strip-like bulge, it is not necessarily that  $H^+$  density should surpass  $O^+$  density, and the strip-like bulge is conformed to appear both below and above the  $O^+/H^+$  transition height.

Note that the optical observations of the neutral winds are made below 300 km (within 250~300 km in this study), while the in-situ observation of the bulges on Ni profiles are made above 430 km (the lowest orbit altitude is 430 km for Swarm A). The direction of the disturbances neutral winds from 300 to 430 km at middle latitudes should be the same, since the upper thermospheric wind circulation is in a global scale, especially during the geomagnetic disturbed period when the heat source comes from the polar region. Therefore, the ICON's neutral wind observation at lower altitudes should be suitable to interpret the ionospheric structure at higher altitudes.

WAN ET AL. 11 of 17



We conclude that the storm-induced disturbance equatorward neutral wind drives the plasma to move equatorward and also upward along the magnetic field line, and this process would be resisted by the gravity at certain lower latitudes. Hence, the poleward boundary of the midlatitude band structure kept moving equatorward and caused the shrinking, and the midlatitude band structure finally evolved into the strip-like bulge. Moreover, we suggest that this scenario could also exist in the daytime. The reasons are: (a) in the event of Sep. 8~9, 2017 storm, the first detection of the bulges was registered in the afternoon sector; (b) the middle-latitude band structure appears at all times of the day though more pronounced (stronger intensity) at 22:00~04:00 LT (Rajesh et al., 2016). Thus, it is reasonable that the daytime midlatitude band structure can experience the same shrinking process to evolve into the strip-like bulge. However, this daytime formation process ought to be harder to monitor due to the much higher background plasma density.

The storm-induced equatorward neutral wind can also carry the nitrogen-enriched airs and decrease the  $O/N_2$  at middle latitudes, this might also contribute to the TEC decrease over the north side of the strip-like bulge. However, this decreased  $O/N_2$  mechanism should prevail in a wide (in meridional dimension) range (e.g., Prölss, 2008) to cause the large-scale negative storm and less likely to leave a strip-like region unaffected. Therefore, we suggested that the negative ionospheric storm caused by the decreased  $O/N_2$  is at least not a decisive factor in generating the strip-like bulge.

## 5.4. Enhanced Fountain Effect

Several previous studies suggested that it is the enhanced fountain effect induced by the disturbance eastward electric field to provides the source plasma (Foster & Coster, 2007; Foster et al., 2005; Horvath & Lovell, 2008; Maruyama et al., 2013; Tsurutani et al., 2004) to form the shoulders/bulges. However, the concurrence of the strip-like bulge with the EIA feature is not always guaranteed. Heelis and Coley (2007) found that the shoulders may occur independently of, and in the absence of, the enhanced EIA, indicating that the enhanced fountain effect is not a necessary condition for the development of strip-like bulge. In this case, the ion drift exhibit equatorward velocity near the strip-like bulge (Figure 7). To some extent, this feature reduced the likelihood of the involvement of the enhanced fountain effect, which should lead to enhanced poleward ion drift. However, the fountain effect would still have worked before the development of the strip-like bulge, and therefore would help to build the midlatitude patch. To examine this scenario, Figure 8 shows the comparative ICON ion drift vector in the magnetic field frame during the same UT interval of 22:00 ~ 02:00 UT from 3 November to 4 November (Figures 8a~8f, corresponding to the storm initial phase right after SSC) and on 2 November to 3 November (Figures 8g~81, set as quiet time reference), over the equatorial region. The ICON orbits in Figures 8a and 8c are the previous orbits of those shown in Figure 7. The light orange shadow covers the QD latitudes within ±5° where the meridional ion drift could be recognized as a proxy of the intensity of the fountain effect as it is basically in the vertical direction.

During 22:00-02:00 UT from 3 November to 4 November (Figures 8a~8f), the positive field-aligned ion drift prevailed in the Pacific-American sector from afternoon to post-sunset and peaked around the sunset. Note this occurred at low latitudes in both the southern and northern hemispheres, suggesting a prevailing northward transequatorial ion transportation. A similar situation can also be found on the previous day (Figures 8g~8l), but with a smaller magnitude. During the concerned period, the transequatorial neutral wind was also northward, that is, from the summer hemisphere to the winter hemisphere, consistent with the quiet time wind circulations. Considering that the period is within the storm initial phase (Figure 1), it is reasonable that the disturbed wind circulation had not propagated to the midlatitude. This summer-to-winter neutral wind that pushed the plasma along the field line may account for the northward ion transportation.

To illustrate the equatorial zonal electric field variation that directly controls the fountain effect, we focus on the meridional ion drift at  $\pm 5^{\circ}$  QD latitudes (shadowed in light orange). During the first pass (Figure 8d), the equatorial meridional ion drift was positive (upward, eastward electric field) in pre-sunset and oscillated between negative and positive in post-sunset with a mean value of about 6 m/s. The second pass (Figure 8e) registered a prevailing negative equatorial meridional ion drift near the sunset, and the mean value was about -18 m/s. The third pass showed a reverse from negative to positive with a mean value of 8 m/s. It can be concluded that during  $22:00 \sim 02:00$  UT, the equatorial zonal electric field had turned westward and recovered eastward. This oscillation might be related to the IMF Bz oscillations (Figure 1b) which allow the penetration of the magnetospheric electric field to the ionosphere (e.g., Kelley et al., 1979; Senior & Blanc, 1984). During the reference days, though

WAN ET AL. 12 of 17

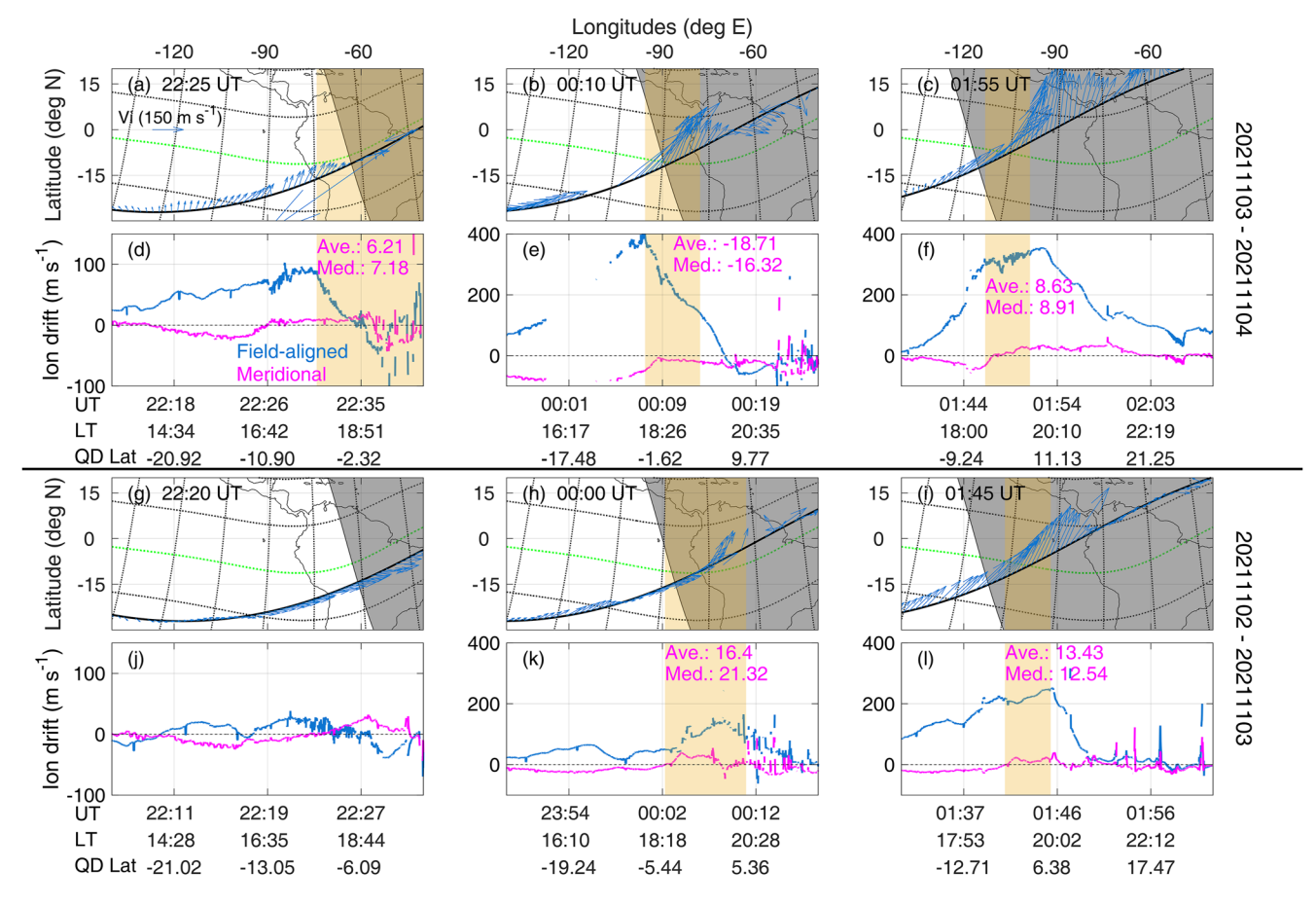


Figure 8. Comparison of ion drift configuration during 22:00-02:00 UT of 3 November-4 November 2021 (a-f) and 2 November-3 November 2021 (g-l), the latter period is set as a quiet time reference. The trajectories and the horizontal ion drift vector in the geographic frame are shown in the same way in Figure 7. The blue and magenta lines in (d-f, j-l) are the ion drift in the geomagnetic frame of the field-aligned (positive along the geomagnetic field vector) and meridional components (within the geomagnetic meridional plane, perpendicular to the field line, positive outward), respectively. The light orange shaded area marks the trajectories section within QD latitude of  $\pm 5^{\circ}$ . The averaged and median values of meridional ion drift within  $\pm 5^{\circ}$  QD latitudes are shown in magenta numbers.

the equatorial meridional ion drift at  $\pm 5^{\circ}$  QD latitudes was not available on the first satellite pass (Figure 8j), the latter two passes did register a stronger positive equatorial meridional ion drift, compared with that of 3 November  $\sim 4$  November. Other evidence had been also noticed by DMSP ion drift data shown in Figure 2. On 4 November at 10:20 UT when the bulge is well-formed, as the field-aligned ion drift showed consistent equatorward velocity in both the northern and southern hemisphere, the  $E \times B$  drifts is rather weak and the polarity varies among the bulge cases, indicating that the  $E \times B$  drifts less like to be involved.

The above observations revealed that the equatorial eastward electric field is not enhanced either in a sense of the short-term temporal evolution or compared with the reference quiet days. Hence, the enhanced fountain effect was not likely to provide the source plasma to form the midlatitude band structure or the strip-like bulge.

# 5.5. Maintenance of the Strip-Like Bulge

The last issue lies in the long-lasting feature of the strip-like bulge (Figure 3), which had even survived during daytime (Wan et al., 2021). As mentioned earlier, the low magnitude of the strip-like bulge makes it hard to be monitored on the TEC map during the daytime. We again focus on the nighttime sector, similar to Figures 7, Figure 9 shows the ICON's measurement overlapped with the TEC maps during  $03:45 \sim 12:20$  UT of 5 November (similar UT interval compared to Figure 7).

During the entire period, the neutral wind was persistently northward corresponding to the summer-to-winter wind scenario. The meridional ion drift also remained northward within the strip-like bulge. During the

WAN ET AL. 13 of 17



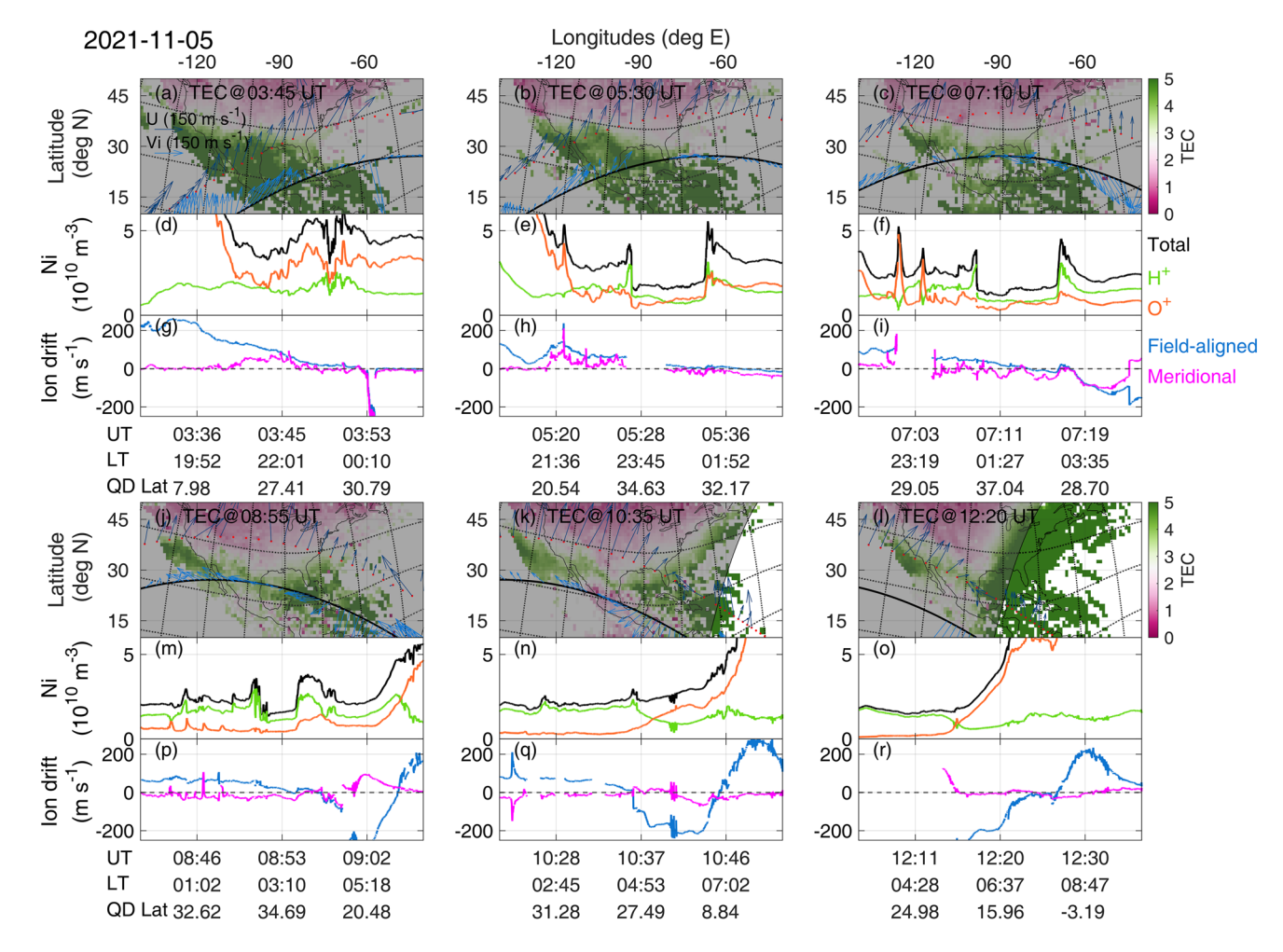


Figure 9. Same as Figure 7 but for the period of 03:30-12:40 UT on 5 November 2021.

concerned periods, it was at about 08:55 UT (Figure 9j) when the TEC map first registered a clear strip-like bulge signature, as a consequence of the TEC decay at lower latitudes (Figures 9a~9c). Focus on the satellite trajectories near the strip-like bulge, the field-aligned ion drift mainly kept downward/poleward (Figures 9h, 9i, 9p, and 9q), and the magnetic meridional component of the ion drifts were in a weak magnitude and mainly kept in an inward direction (Figures 9i, 9p, and 9q). Therefore, unlike the synchronous turning of the ion drifts regards to the first emergence of the strip-like bulge on 4 November (Figure 7), the ion drift showed no corresponding variations on 5 November, suggesting that the reemergence of the strip-like bulge is not associated with the ion drifts.

The question should be raised as how the strip-like bulge reemerged on 5 November. Please note that though the TEC maps failed to capture the strip-like bulge features before 08:55 UT (Figures  $9a \sim 9c$ ), it does not mean that the strip-like bulge did not exist before this reemergence. According to the results of Wan et al. (2021), the LEO satellites can track bulge signals at almost all local times. In this case, indirect evidence can be found on the ion composition profiles. Before and after the first emergence of distinctive bulge features, the TEC exhibited scraggy distribution (Figures 9b, c9j, and 9k), correspondingly, multiple peaks can be found on the ICON ion density profiles (Figures 9e, 9f, 9m, and 9n). Among those peaks, some were dominated by  $O^+$  (two peaks on the left of Figure 9f) and the rest were dominated by  $H^+$ . The  $O^+$  dominated peaks are likely the blobs (e.g., Park et al., 2022), while the rest  $H^+$  dominated peaks should be the zonal snapshots of the strip-like bulge. Thus, we emphasize that the strip-like bulge was likely maintained in a long time interval and residing in a relative fixed location, and the retreat of TEC at lower latitudes (compared to the latitudes of the bulges) made the bulge observable on the TEC maps.

WAN ET AL. 14 of 17



Figure 9d and the low latitude portion of Figures 9m-9o show that the  $O^+$  was the major contributor to the total ion density. The recombination of  $O^+$  and electrons would reduce the TEC in the  $O^+$  dominated region, which could be the cause of the retreat of TEC at lower latitudes. Nevertheless, the production and loss of  $H^+$  can be characterized by the charge exchange reaction of  $O^+ + H \leftrightarrow H^+ + O$  (Prölss, 2004). On the one hand, the charge exchange does not affect the total electron number or TEC, in the current circumstance, the northern portion (higher percentage of  $H^+$ ) of the "scraggy patch" is maintained during the night while the TEC of the southern portion (higher percentage of  $O^+$ ) decayed, therefore the strip-like bulge reemerged on TEC maps (Figures 6 and 9). On the other hand,  $H^+$  density exceeded the  $O^+$  density in the vicinity of the strip-like bulge/plasma band structure (Figures 7a, 7d, and 7j), indicating that the transition height between  $O^+/H^+$  was below the ICON's altitude, and the diffusive equilibrium of H<sup>+</sup> should be considered (Lemaire & Gringauz, 1998, pp. 166–167). Besides, the midlatitude band structure, which is believed to be created by the downward plasmaspheric flux, can be found through the day and night (Rajesh et al., 2016), indicating a possible persistent supply of  $H^+$  from the plasmasphere to the topside ionosphere. Hence, the  $H^+$  chemical loss due to the fast charge exchange reaction (the chemical equilibrium) should be compensated by the sustainable supply of H<sup>+</sup> from the plasmasphere, which may account for the long-lasting feature of the strip-like bulge. We acknowledge that plasmaspheric particle compensation mechanism still faces some limitations: (a) how the process sustained during the daytime; (b) why this works preferentially at narrow latitude of strip-like bulge and not to smooth the bulge out. Further dedicated plasmasphere-ionosphere coupling simulations in the future is needed.

## 6. Conclusions

During the geomagnetic storm on 3–6 November 2021, the gridded TEC maps, for the first time, exhibited a full evolution process of the strip-like bulge over North America. By including satellite observations from Swarm A, B, DMSP F16, F17, F18, and ICON, a few important aspects concerning the development and maintenance of the strip-like bulge had been revealed. The main findings are summarized below:

- 1. In-situ plasma density profiles collected by the five high-inclination satellites had persistently snapshotted the strip-like bulge over the Pacific-America-Atlantic sector from 07:00 UT of 4 November to 20:00 UT of 6 November, covering the storm main phase and recovery phase.
- 2. The TEC map had registered the emergence process of the strip-like bulge feature on both nights of 4 November and 5 November. On 4 November, the continuous shrinking of TEC patch converted the midlatitude plasma band structure into the strip-like bulge. On 5 November, the ICON ion composition data confirmed the persistence of the strip-like bulge though it was not registered on TEC maps at first. After the following decay of TEC at lower latitudes and the maintenance of TEC at higher latitudes, the strip-like bulge became distinguishable on TEC maps.
- 3. The shrinking/narrowing of the midlatitude plasma band structure (the formation of the strip-like bulge) is due to the enhanced equatorward ion transportation along the field lines driven by the disturbance equatorward neutral winds. In other words, the strip-like bulge is the storm time shrunken midlatitude plasma band structure.
- 4. The enhanced fountain effect at equatorial and low latitudes is not involved in supplying the plasma or helping to form the strip-like bulge.
- 5. The maintenance of the strip-like bulge might be associated with its  $H^+$  abundance nature that the chemical loss via charge exchange reaction could be compensated by the downward plasmaspheric content flux.

# **Data Availability Statement**

Swarm data are provided by the European Space Agent (https://earth.esa.int/web/guest/swarm/data-access). DMSP data are provided by the National Centers for Environmental Information (https://satdat.ngdc.noaa.gov/dmsp/). ICON data can be accessed at the ICON Science Data Center at University of California, Berkeley (https://icon.ssl.berkeley.edu/Data/Data-Product-Matrix). The solar wind and geomagnetic indices can be accessed in the GSFC/SPDF OMNIWeb database (https://omniweb.gsfc.nasa.gov/). *Kp* is provided by the Kyoto World Data Center for Geomagnetism (http://wdc.kugi.kyoto-u.ac.jp/index.html). The gridded GPS TEC data are provided by the CEDAR Madrigal database (http://cedar.openmadrigal.org/ftp/). IGRF-13 coefficients are provided by the International Association of Geomagnetism and Aeronomy (https://www.ngdc.noaa.gov/IAGA/vmod/igrf.html).

WAN ET AL. 15 of 17



#### Acknowledgments

This work was supported by the Strategic Priority Research Program of Chinese Academy of Sciences (XDB41000000), the National Natural Science Foundation of China (41831070, 42104169, 41804150, 42104147, 41804153, 42164010, 42004136), China Postdoctoral Science Foundation (2020M683025), Guangdong Basic and Applied Basic Research Foundation (2022A1515011580. 2021A1515011216, 2020A1515110242), Hubei Province Outstanding Youth Project (2017CFA057), the Natural Science Foundation of Jiangsu Province (BK20180445), Joint Open Fund of Mengcheng National Geophysical Observatory (MENGO-202217), the Fundamental Research Funds for the Central Universities, the Opening Funding of Chinese Academy of Sciences dedicated for the Chinese Meridian Project, the Open Research Project of Large Research Infrastructures of CAS—"Study on the interaction between low/mid-latitude atmosphere and ionosphere based on the Chinese Meridian Project." GNSS TEC data products and access through the Madrigal distributed data system are provided to the community by the Massachusetts Institute of Technology under support from US National Science Foundation grant AGS-1952737. Work at MIT was partially supported by AFOSR MURI grant FA9559-16-1-0364 and NSF grant AGS-2033787.

## References

- Aa, E., Huang, W., Liu, S., Ridley, A., Zou, S., Shi, L., et al. (2018). Midlatitude plasma bubbles over China and adjacent areas during a magnetic storm on 8 September 2017. Space Weather, 16, 321–331. https://doi.org/10.1002/2017SW001776
- Alken, P., Thébault, E., Beggan, C. D., Amit, H., Aubert, J., Baerenzung, J., et al. (2021). International geomagnetic reference field: The thirteenth generation. *Earth Planets and Space*, 73, 49. https://doi.org/10.1186/s40623-020-01288-x
- Balan, N., Shiokawa, K., Otsuka, Y., Kikuchi, T., Lekshmi, D. V., Kawamura, S., et al. (2010). A physical mechanism of positive ionospheric storms at low latitudes and midlatitudes. *Journal of Geophysical Research*, 115(A2), A02304. https://doi.org/10.1029/2009JA014515
- Carter, B. A., Retterer, J. M., Yizengaw, E., Wiens, K., Wing, S., Groves, K., et al. (2014). Using solar wind data to predict daily GPS scintillation occurrence in the African and Asian low-latitude regions. *Geophysical Research Letters*, 41, 8176–8184. https://doi.org/10.1002/2014GL062203
- Carter, B. A., Yizengaw, E., Pradipta, R., Retterer, J. M., Groves, K., Valladares, C., et al. (2016). Global equatorial plasma bubble occurrence during the 2015 St. Patrick's Day storm. *Journal of Geophysical Research: Space Physics*, 121, 894–905. https://doi.org/10.1002/2015JA022194
- Chartier, A. T., Datta-Barua, S., McDonald, S. E., Bust, G. S., Tate, J., Goncharenko, L. P., et al. (2021). Night-time ionospheric localized enhancements (NILE) observed in North America following geomagnetic disturbances. *Journal of Geophysical Research: Space Physics*, 126, e2021JA029324. https://doi.org/10.1029/2021JA029324
- Coster, A. J., Colerico, M. J., Foster, J. C., Rideout, W., & Rich, F. (2007). Longitude sector comparisons of storm enhanced density. *Geophysical Research Letters*, 34, L18105. https://doi.org/10.1029/2007gl030682
- Datta-Barua, S., Mannucci, A. J., Walter, T., & Enge, P. (2008). Altitudinal variation of midlatitude localized TEC enhancement from ground- and space-based measurements. Space Weather, 6, S10D06. https://doi.org/10.1029/2008SW000396
- Emmert, J. T., Fejer, B. G., Fesen, C. G., Shepherd, G. G., & Solheim, B. H. (2001). Climatology of middle- and low-latitude daytime F region disturbance neutral winds measured by Wind Imaging Interferometer (WINDII). *Journal of Geophysical Research*, 106(A11), 24701–24712. https://doi.org/10.1029/2000JA000372
- Fejer, B. G., Emmert, J. T., Shepherd, G. G., & Solheim, B. H. (2000). Average daytime F region disturbance neutral winds measured by UARS: Initial results. *Geophysical Research Letters*, 27(13), 1859–1862. https://doi.org/10.1029/2000GL003787
- Foster, J. C. (1993). Storm time plasma transport at middle and high latitudes. *Journal of Geophysical Research*, 98(A2), 1675–1689. https://doi.org/10.1029/92JA02032
- Foster, J. C., & Coster, A. J. (2007). Conjugate localized enhancement of total electron content at low latitudes in the American sector. *Journal of Atmospheric and Solar-Terrestrial Physics*, 69, 1241–1252. https://doi.org/10.1016/j.jastp.2006.09.012
- Foster, J. C., Coster, A. J., Erickson, P. J., Holt, J. M., Lind, F. D., Rideout, W., et al. (2005). Multiradar observations of the polar tongue of ionization. *Journal of Geophysical Research*, 110, A09S31. https://doi.org/10.1029/2004JA010928
- Foster, J. C., & Erickson, P. J. (2013). Ionospheric superstorms: Polarization terminator effects in the Atlantic sector. *Journal of Atmospheric and Solar-Terrestrial Physics*, 103, 147–156. https://doi.org/10.1016/j.jastp.2013.04.001
- Foster, J. C., Rideout, W., Sandel, B., Forrester, W. T., & Rich, F. J. (2007). On the relationship of SAPS to storm-enhanced density. *Journal of Atmospheric and Solar-Terrestrial Physics*, 69(3), 303–313. https://doi.org/10.1016/j.jastp.2006.07.021
- Friis-Christensen, E., Lühr, H., Knudsen, D., & Haagmans, R. (2008). Swarm—An Earth observation mission investigating geospace. Advances in Space Research, 41(1), 210–216. https://doi.org/10.1016/j.asr.2006.10.008
- Harding, B., Makela, J., Englert, C., Marr, K. D., Harlander, M., England, S. L., & Immel, T. (2017). The MIGHTI wind retrieval algorithm: Description and verification. *Space Science Reviews*, 212, 585–600. https://doi.org/10.1007/s11214-017-0359-3
- Heelis, R. A., & Coley, W. R. (2007). Variations in the low- and middle-latitude topside ion concentration observed by DMSP during superstorm events. *Journal of Geophysical Research*, 112, A08310. https://doi.org/10.1029/2007JA012326
- Heelis, R. A., Stoneback, R. A., Perdue, M. D., Depew, M. D., Morgan, W. A., Mankey, M. W., et al. (2017). Ion velocity measurements for the ionospheric connections explorer. *Space Science Reviews*, 212, 615–629. https://doi.org/10.1007/s11214-017-0383-3
- Horvath, I., & Lovell, B. C. (2008). Formation and evolution of the ionospheric plasma density shoulder and its relationship to the superfountain effects investigated during the 6 November 2001 great storm. *Journal of Geophysical Research*, 113, A12315. https://doi.org/10.1029/2008JA013153
- Immel, T. J., England, S. L., Mende, S. B., Heelis, R. A., Englert, C. R., Edelstein, J., et al. (2018). The ionospheric connection explorer mission: Mission goals and design. Space Science Reviews, 214, 13. https://doi.org/10.1007/s11214-017-0449-2
- Kelley, M. C., Fejer, B. G., & Gonzales, C. A. (1979). An explanation for anomalous equatorial ionospheric electric fields associated with a northward turning of the interplanetary magnetic field. *Geophysical Research Letters*, 6, 301–304. https://doi.org/10.1029/GL006i004p00301
- Kelley, M. C., Vlasov, M. N., Foster, J. C., & Coster, A. J. (2004). A quantitative explanation for the phenomenon known as storm-enhanced density. Geophysical Research Letters, 31, L19809. https://doi.org/10.1029/2004GL020875
- Lemaire, J., Gringauz, K., Carpenter, D. L., & Bassolo, V. (1998). The Earth's plasmasphere. Cambridge University Press. https://doi.org/10.1017/CBO9780511600098
- Li, Q., Hao, Y., Zhang, D., & Xiao, Z. (2018). Nighttime enhancements in the midlatitude ionosphere and their relation to the plasmasphere. Journal of Geophysical Research: Space Physics, 123, 7686–7696. https://doi.org/10.1029/2018JA025422
- Lin, C. H., Richmond, A. D., Heelis, R. A., Bailey, G. J., Lu, G., Liu, J. Y., et al. (2005). Theoretical study of the low- and midlatitude ionospheric electron density enhancement during the October 2003 superstorm: Relative importance of the neutral wind and the electric field. *Journal of Geophysical Research*, 110, A12312. https://doi.org/10.1029/2005JA011304
- Mannucci, A. J., Tsurutani, B. T., Iijima, B. A., Komjathy, A., Saito, A., Gonzalez, W. D., et al. (2005). Dayside global ionospheric response to the major interplanetary events of October 29-30, 2003 "Halloween storms. Geophysical Research Letters, 32(12), L12S02. https://doi. org/10.1029/2004GL021467
- Maruyama, T., Ma, G., & Tsugawa, T. (2013). Storm-induced plasma stream in the low-latitude to midlatitude ionosphere. *Journal of Geophysical Research: Space Physics*, 118, 5931–5941. https://doi.org/10.1002/jgra.50541
- Park, J., Huang, C.-S., Eastes, R. W., & Coster, A. J. (2022). Temporal evolution of low-latitude plasma blobs identified from multiple measurements: ICON, GOLD, and Madrigal TEC. *Journal of Geophysical Research: Space Physics*, 127, e2021JA029992. https://doi. org/10.1029/2021JA029992
- Prölss, G. W. (2004). Physics of the earth's space environment: An introduction (pp. 168–171). Springer. https://doi.org/10.1007/978-3-642-97123-5\_3
  Prölss, G. W. (2008). Ionospheric storms at mid-latitude: A short review. In P. M. Kintner (Ed.), Midlatitude ionospheric dynamics and disturbances, Geophysical monograph series (Vol. 181, pp. 9–24). AGU. https://doi.org/10.1029/181GM03
- Rajesh, P. K., Liu, J. Y., Balan, N., Lin, C. H., Sun, Y. Y., & Pulinets, S. A. (2016). Morphology of midlatitude electron density enhancement using total electron content measurements. *Journal of Geophysical Research: Space Physics*, 121, 1503–1517. https://doi.org/10.1002/2015JA022251

WAN ET AL. 16 of 17



- Rideout, W., & Coster, A. (2006). Automated GPS processing for global total electron content data. GPS Solutions, 10, 219–228. https://doi.org/10.1007/s10291-006-0029-5
- Senior, C., & Blanc, M. (1984). On the control of magnetospheric convection by the spatial distribution of ionospheric conductivity. *Journal of Geophysical Research*, 89, 261–284. https://doi.org/10.1029/ja089ia01p00261
- Tsurutani, B., Mannucci, A., Iijima, B., Abdu, M. A., Sobral, J. H. A., Gonzalez, W., et al. (2004). Global dayside ionospheric uplift and enhancement associated with interplanetary electric fields. *Journal of Geophysical Research*, 109, A08302. https://doi.org/10.1029/2003JA010342
- Vlasov, M., Kelley, M. C., & Kil, H. (2003). Analysis of ground-based and satellite observations of F-region behavior during the great magnetic storm of July 15, 2000. Journal of Atmospheric and Solar-Terrestrial Physics, 65, 1223–1234. https://doi.org/10.1016/j.jastp.2003.08.012
- Wan, X., Xiong, C., Rodriguez-Zuluaga, J., Kervalishvili, G. N., Stolle, C., & Wang, H. (2018). Climatology of the occurrence rate and amplitudes of local time distinguished equatorial plasma depletions observed by Swarm satellite. *Journal of Geophysical Research: Space Physics*, 123, 3014–3026. https://doi.org/10.1002/2017JA025072
- Wan, X., Xiong, C., Wang, H., Zhang, K., & Yin, F. (2020). Spatial characteristics on the occurrence of the nighttime midlatitude medium-scale traveling ionospheric disturbance at topside ionosphere revealed by the Swarm satellite. *Journal of Geophysical Research: Space Physics*, 125, e2019JA027739. https://doi.org/10.1029/2019JA027739
- Wan, X., Zhong, J., Xiong, C., Wang, H., Liu, Y., Li, Q., et al. (2021). Persistent occurrence of strip-like plasma density bulges at conjugate lower-mid latitudes during the September 8–9, 2017 geomagnetic storm. *Journal of Geophysical Research: Space Physics*, 126, e2020JA029020. https://doi.org/10.1029/2020JA029020
- Wang, H., Zhang, K. D., Wan, X., & Lühr, H. (2017). Universal time variation of high-latitude thermospheric disturbance wind in response to a substorm. *Journal of Geophysical Research: Space Physics*, 122, 4638–4653. https://doi.org/10.1002/2016JA023630
- Xiong, C., Lin, F., Luo, X., Jin, Y., & Wan, X. (2019). Plasma patches inside the polar cap and auroral oval: The impact on the spaceborne GPS receiver. *Journal of Space Weather and Space Climate*, 9, A25. https://doi.org/10.1051/swsc/2019028
- Xiong, C., Lühr, H., & Fejer, B. G. (2015). Global features of the disturbance winds during storm time deduced from CHAMP observations. Journal of Geophysical Research: Space Physics, 120, 5137–5150. https://doi.org/10.1002/2015JA021302
- Xiong, C., Lühr, H., Sun, L., Luo, W., Park, J., & Hong, Y. (2019). Long-lasting latitudinal four-peak structure in the nighttime ionosphere observed by the Swarm constellation. *Journal of Geophysical Research: Space Physics*, 124, 9335–9347. https://doi.org/10.1029/2019JA027096
- Xiong, C., Stolle, C., & Lühr, H. (2016). The Swarm satellite loss of GPS signal and its relation to ionospheric plasma irregularities. Space Weather, 14, 563–577. https://doi.org/10.1002/2016SW001439
- Yeh, H. C., Su, S. Y., & Heelis, R. A. (2001). Storm time plasma irregularities in the pre-dawn hours observed by the low-latitude ROCSAT-1 satellite at 600 km. Geophysical Research Letters, 28(4), 685–688. https://doi.org/10.1029/2000GL012183
- Zakharenkova, I., & Cherniak, I. (2020). When plasma streams tie up equatorial plasma irregularities with auroral ones. Space Weather, 18, e2019SW002375. https://doi.org/10.1029/2019SW002375
- Zakharenkova, I., & Cherniak, I. (2021). Effects of storm-induced equatorial plasma bubbles on GPS-based kinematic positioning at equatorial and middle latitudes during the September 7–8, 2017, geomagnetic storm. GPS Solutions, 25, 132. https://doi.org/10.1007/s10291-021-01166-3
- Zhang, K., Wang, H., Liu, J., Zheng, Z., He, Y., Gao, J., et al. (2021). Dynamics of the tongue of ionizations during the geomagnetic storm on September 7, 2015. *Journal of Geophysical Research: Space Physics*, 126, e2020JA029038. https://doi.org/10.1029/2020JA029038
- Zhang, Q.-H., Zhang, B.-C., Moen, J., Lockwood, M., McCrea, I. W., Yang, H.-G., et al. (2013). Polar cap patch segmentation of the tongue of ionization in the morning convection cell. *Geophysical Research Letters*, 40, 2918–2922. https://doi.org/10.1002/grl.50616
- Zhang, S.-R., Erickson, P. J., Zhang, Y., Wang, W., Huang, C., Coster, A. J., et al. (2017). Observations of ion-neutral coupling associated with strong electrodynamic disturbances during the 2015 St. Patrick's Day storm. *Journal of Geophysical Research: Space Physics*, 122(1), 1314–1337. https://doi.org/10.1002/2016JA023307
- Zhong, J., Lei, J., Yue, X., Luan, X., & Dou, X. (2019). Middle-latitudinal band structure observed in the nighttime ionosphere. *Journal of Geophysical Research: Space Physics*, 124, 5857–5873. https://doi.org/10.1029/2018JA026059

WAN ET AL. 17 of 17